INFLUENCE OF CURVATURE ON DRAG REDUCTION BY OPPOSITION CONTROL IN TURBULENT FLOW ALONG A THIN CYLINDER

Shota Hara, Hiroya Mamori, Takeshi Miyazaki
Department of Mechanical and Intelligent Systems Engineering
The University of Electro-Communications
1-5-1, Chofugaoka, Chofu, Tokyo, Japan, 182-8585
mamori@uec.ac.jp

ABSTRACT

Opposition controlled fully developed turbulent flows along a thin cylinder are performed by means of direct numerical simulations. An influence of cylinder curvature on the skin-friction drag reduction effect by the classical opposition control (i.e., the radial velocity control) is mainly investigated. The curvature of cylinder affects the uncontrolled flow statistics; however, the control effect in the small curvature case is similar to that in channel flow. In the case where the curvature is large, drag reduction rates are obtained at the high detection plane and these are larger than those in the channel flow.

INTRODUCTION

Flow control to decrease skin-friction drag in turbulent flows is of importance in mitigating the environmental impact. To decrease the wall-turbulence, many control techniques are examined numerically and experimentally.

The turbulent flows along the cylinders are important from viewpoints of the engineering e.g., ship hulls, aircraft fuselage, sonar array, and monofilament yarn. It is known that due the curvature of the cylinder the skin-friction drag coefficient differs from that of the flat plate and there are two parameters to characterize the flow: $\gamma\,(=\delta/a)$ and a^+. Here δ is the boundary layer thickness and a is the cylinder radius. The superscripts of the plus means the wall units. Piquet & Patal (1999) and Afzal & Narasimha (1985) categorized the effect of the curvature on the flow:

- at $\gamma \lesssim 1$ and $a^+ \gtrsim 250$, an influence of curvature is very small;
- at $\gamma \gg 1$ and $a^+ \gtrsim 250$, curvature affects the outer layer;
- at $\gamma \gg 1$ and $a^+ \lesssim 250$, curvature affects not only the outer layer, but also the inner layer.

In addition, there are many investigations of uncontrolled turbulent flows along a thin cylinder (e.g. Ohta, 2017). However, the control aiming to decrease the skin-friction drag has not been examined yet in the turbulent flow along the thin cylinder.

In this study, we perform the controlled turbulent flows along the cylinder by means of direct numerical simulations (referred as DNS, hereafter) and investigate the influence of the curvature on the drag reduction effect. As the turbulent flow control, we employ classical opposition control technique (i.e., the so-called *v*-control, Choi *et al.* (1994)) for the simplicity.

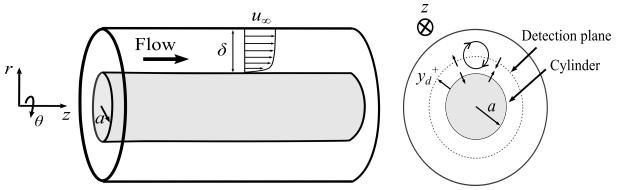

Figure 1: Schematic of the opposition controlled flow along a thin cylinder.

Numerical Simulation

We perform the DNS of the flow along the cylinder. The governing equations are incompressible continuity and Navier-Stokes equations in a cylindrical coordinate system. The continuity equation is

$$\frac{1}{r}\frac{\partial}{\partial r}(ru_r)+\frac{1}{r}\frac{\partial u_\theta}{\partial \theta}+\frac{\partial u_z}{\partial z}=0, \tag{1}$$

where u is the velocity and the subscripts of r, θ, and z mean the radial, azimuthal, and streamwise directions, respectively. The Navier-Stokes equations are

$$\frac{\partial u_r}{\partial t}=h_r-\frac{\partial p}{\partial r}+\frac{1}{\mathrm{Re}_\tau}d_r, \tag{2}$$

$$\frac{\partial u_\theta}{\partial t}=h_\theta-\frac{1}{r}\frac{\partial p}{\partial \theta}+\frac{1}{\mathrm{Re}_\tau}d_\theta, \tag{3}$$

$$\frac{\partial u_z}{\partial t}=h_z-\frac{\partial p}{\partial z}+\frac{1}{\mathrm{Re}_\tau}d_z. \tag{4}$$

Here, t is the time, p is the pressure, h is the convection terms, and d is the diffusion term. The reference velocity and length are the friction velocity u_τ^* and the boundary layer thickness δ^*, respectively. The asterisk denotes the dimensional variable. The skin-friction Reynolds number of Re_τ is set 180, 214 and 235 for γ = 0, 5 and 11, respectively. The skin-friction Reynolds number corresponds to that based on the the boundary layer thickness and the free-stream velocity of 3400 for uncontrolled case. The

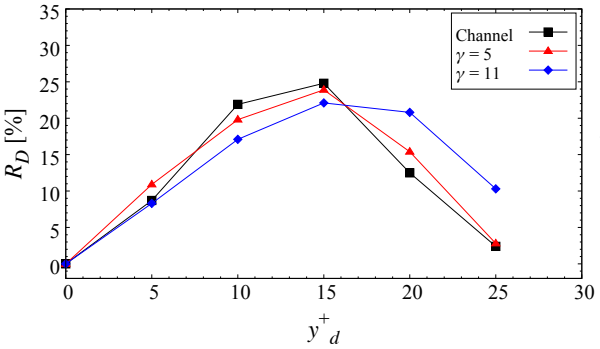

Figure 2: Drag reduction rate R_D as a function of location of the detection plane.

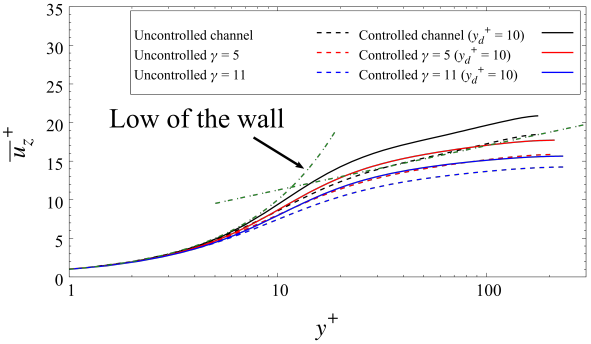

Figure 3: Mean streamwise velocity profiles.

DNS code is based on that by Fukagata & Kasagi (2002): the governing equations are spatially discretized using the finite-difference method with a second-order central differencing scheme; as for the time advance, the second-order Crank-Nicolson scheme is employed for the viscous terms and low-storage third-order Runge-Kutta scheme is employed for the other terms.

Figure 1 shows a schematic of the opposition controlled flow along the thin cylinder. The computational domain is $L_z^+ \approx 4000$ in the streamwise diection and $\delta = 1$ in the radial direction. The number of grid points is $N_r \times N_\theta \times N_z = 96 \times 128 \times 320$. The curvature ratio of γ are 5 and 11. As comparison, the turbulent channel flow is also simulated as $\gamma = 0$. In the present channel flow case, the computational domain is $L_x = 2\pi$ in the streamwise direction and $L_z = \pi$ in the spanwise direction, and the number of grid points is $N_x \times N_y \times N_z = 128 \times 96 \times 128$, and the skin-friction Reynolds number based on the half channel width is set 180.

The periodic condition is imposed in the streamwise direction. At the outer boundary of the computational domain, we imposed,

$$\frac{\partial}{\partial r}\left(\frac{u_\theta}{r}\right) = \frac{\partial u_z}{\partial r} = 0, \quad u_r = 0. \tag{5}$$

On the cylinder surface, a no-slip condition is imposed in the uncontrolled case, whereas the wall-velocity is imposed in the controlled cases as

$$u_{r,\,w} = -u_{r,\,y_d^+}. \tag{6}$$

The $u_{r,\,w}$ corresponds to the v-control in the channel flow case (Choi *et al.*, 1994), and y_d^+ is the location of the detection plane ($y_d^+ = (r-a)^+$). The subscript of w means the wall value. We examine the radial u_r-control with five different detection planes of $y_d^+ = 5$, 10, 15, 20, and 25.

All the simulations start from a fully developed turbulent flow along the thin cylinder. Since the mean pressure gradient in the streamwise direction ($-\partial P/\partial z = 2a/(2a+1)$) is kept constant, the drag reduction effect corresponds to the increase in the bulk flow rate.

The cost functions are the skin-friction coefficient C_f and the drag reduction rate R_D, as

$$C_f = \frac{\tau_w^*}{\frac{1}{2}\rho^* u_\infty^{*2}}, \quad R_D = \frac{C_{f0} - C_f}{C_{f0}}, \tag{7}$$

respectively. Here, τ_w^* denotes the wall shear stress. The subscript of zero means the uncontrolled flow.

Results

Figure 2 shows the drag reduction rate R_D as a function of y_d^+. The drag reduction rate of the radial control peaks at $y_d^+ = 15$ for all the cases, while these are smaller than that of the channel flow case: the maximum drag reduction rate by the v-control was about 25% (present study and Choi *et al.* (1994)). As increasing the height of the detection plane, the drag reduction rate decreases for both the cylinder and channel flow cases. However, 10% of the drag reduction rate is obtained at $\gamma = 11$ and $y_d^+ = 25$. It implies that the drag reduction rates can be obtained at the higher detection plane in the large curvature cylinder case. In the following, we chose the location of the detection plane $y_d^+ = 10$ as for the reference.

Figure 3 shows the mean streamwise velocity profile and Fig. 4 shows the Reynolds shear stress (RSS, $-\overline{u_r' u_z'}$) and the rms values of the velocities. In the uncontrolled case, the mean velocity, the RSS, and the rms value decrease in increase of the curvature of the cylinder (Neves *et al.*, 1992; Woods, 2006). In the controlled case, in contrast, the mean velocity increases, while the RSS and the rms value decrease. The decrease of the rms values in the region near the cylinder surface shows a similar trend to that in the controlled channel flow. Because the RSS plays an important role in the skin-friction coefficient, the reduction of the RSS contributes to the decrease of the skin-friction coefficient (Fukagata *et al.*, 2002; Monte *et al.*, 2011).

The skin-friction coefficient of the turbulent contribution is identical to the integration of the weighted RSS, as

$$C_{f,turb.} = \frac{1}{f(a)} \int_a^{a+1} (1+a-r)(-\overline{u_r' u_z'}) r dr. \tag{8}$$

Here, $f(a) = -a(1/24 + a/6)/(2a+1) + a/4$ is a the shape factor of the cylindrical geometry. The weighted RSS is

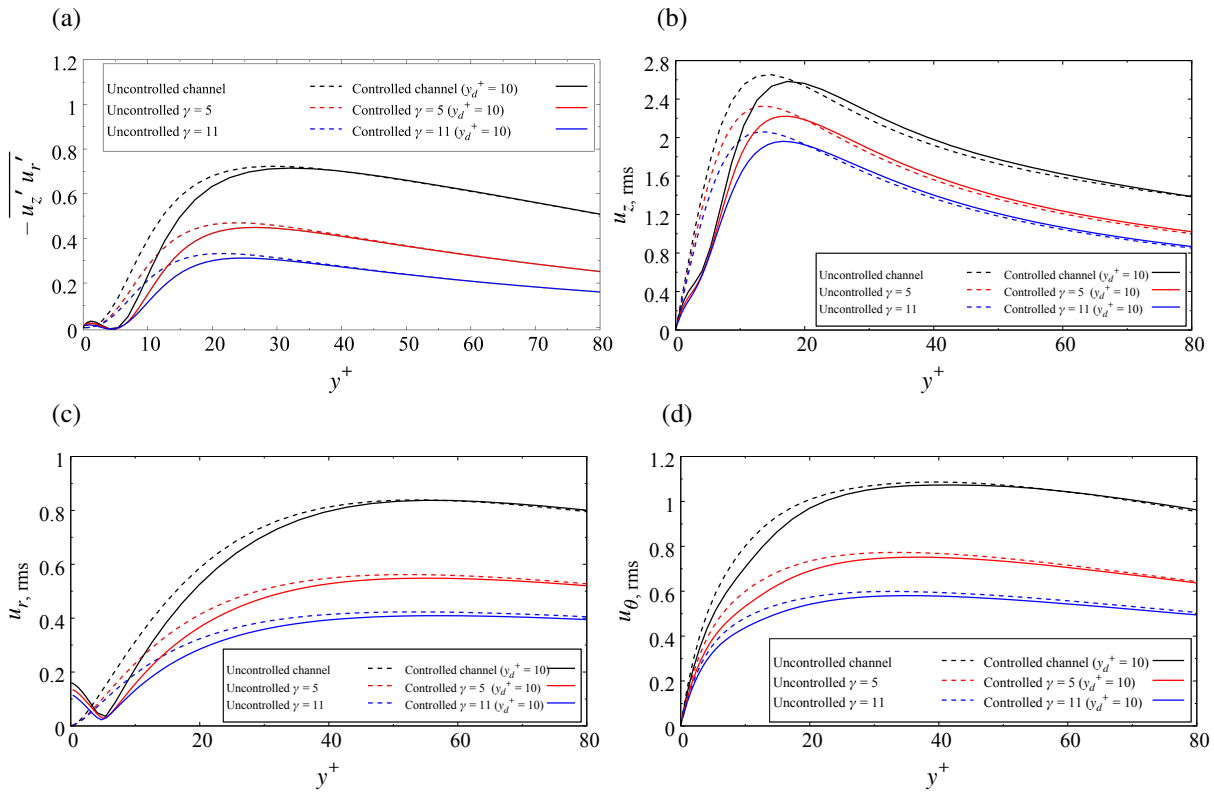

Figure 4: Profile of (a) the Reynolds shear stress, the rms value of (b) streamwise, (c) radial, and (d) azimuthal velocity components.

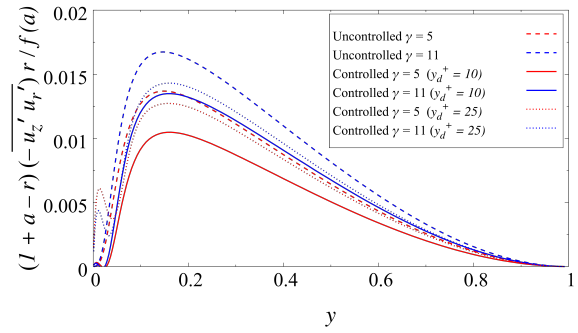

Figure 5: Distributions of the weighted Reynolds shear stress.

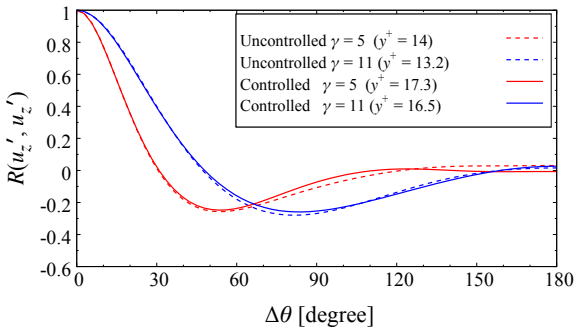

Figure 6: Two point correlation of the streamwise velocity fluctuation in the azimuthal diretion.

shown in Fig. 5. In contrast to the RSS distribution, as increase of the curvature, the weighted RSS increases because $f(a)$ decreases, and it results in the increase of the skin-friction drag coefficient. In the controlled cases, since the blowing and suction creates the RSS in the region near the wall, the small weighted-RSS appears. In the case of $\gamma = 5$, the increment cancels out the decrement of the weighted-RSS; it results in the small drag reduction rate. On the other hand, in the case of $\gamma = 11$, the increment of the weighted-RSS in the region near the wall is smaller than the decrement of the weighted-RSS. Therefore, the drag reduction effect can be obtained at the higher detection plane.

Figure 6 shows the two point correlation of the streamwise velocity $R(u_z', u_z')$ in the azimuthal direction. The two point correlation is computed where the rms value of the streamwise velocity peaks for each cases. The minimum peak of $R(u_z', u_z')$ corresponds a space of streaky structures of the velocity. In the case of $\gamma = 5$, the local minimum of $R(u_z', u_z')$ is at 50° and it indicates three or four pairs of the streaky structures. In the case of $\gamma = 11$, since the local minimum is at 80°, there are two or three pairs. However, because the two-point correlation is almost unchanged in the control cases, the control does not affect the number of pairs of the streaky structures, which is similar to that in channel flow (Choi *et al.*, 1994).

Figure 7 shows the instantaneous streamwise velocity fluctuations at $z = L_z/2$. Since the increase in the curvature of the cylinder weakens the turbulence intensity, the streamwise velocity fluctuations in the case of $\gamma = 11$ are smaller than those in case of $\gamma = 5$. In the controlled case, the streamwise vortical structures are suppressed as compared with the uncontrolled case. As shown in Fig. 7(a) and (c), the number of pairs of the streaky structures changes with the curvature in the uncontrolled case (Ohta, 2017).

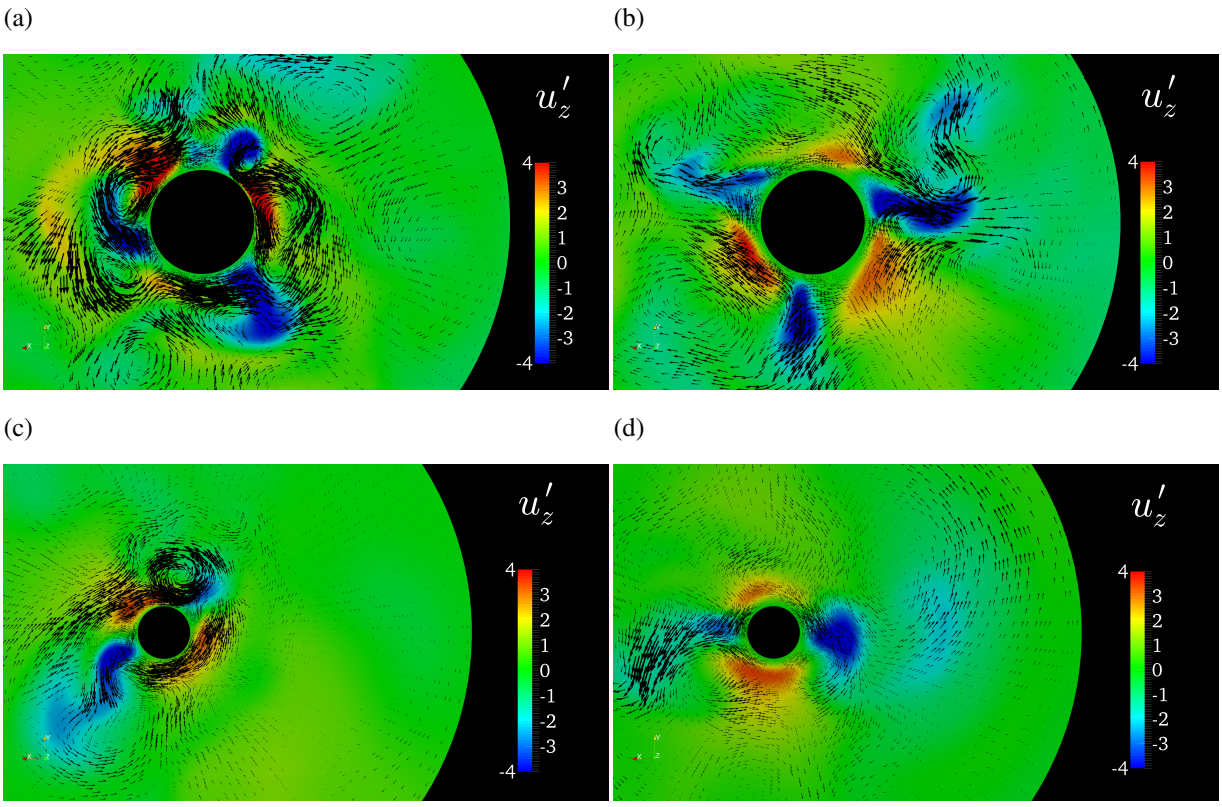

Figure 7: Instantaneous streamwise velocity fluctuations at $z = L_z/2$, (a) uncontrolled case ($\gamma = 5$), (b) controlled case with $y_d^+ = 10$ ($\gamma = 5$), (c) uncontrolled case ($\gamma = 11$), (d) controlled case with $y_d^+ = 10$ ($\gamma = 11$).

However, the number of pairs is unchanged in the controlled flow, which is consistent with Fig.6.

Conclusion

We performed the DNS of turbulence flows along the thin cylinder with the classical opposition control techniques: the radial velocity detecting at the near the wall is imposed on the cylinder surface to cancel out the near wall vortical structures. The drag reduction effect is obtained, while the maximum drag reduction rate is lower than that in the channel flow. For the small curvature case and the channel flow, the drag reduction effect decreases as increase of the height of the detection plane. However, in the case of the curvature of $\gamma = 11$, the drag reduction effect is sustained even at $y_d^+ = 25$. It is because the balance of the near wall peak and the decrement of the RSS: the decrement of the RSS is larger than that of the near wall peak of the RSS at $\gamma = 11$, results in the drag reduction at $y_d^+ = 25$.

Acknowledgments

This research was partially supported by the Ministry of Education, Culture, Sports, Science, and Technology through a Grant-in-Aid for Scientific Research (A) of JP18H03758 in 2019.

REFERENCES

Afzal, N. & Narasimha, R. 1985 Asymtotic analysis of thick axisymmetric turbulent boundary layer. *AIAA J.* **23(6)**, 963–965.

Choi, P., Moin, P. & Kim, J. 1994 Active turbulence control for drag reduction in wall-bounded flows. *J. Fluid Mech.* **262**, 75–110.

Fukagata, K., Iwamoto, K. & Kasagi, N. 2002 Contribution of Reynolds stress distribution to the skin friction in wall-bounded flows. *Phys. Fluids* **14** (11), L73–L76.

Fukagata, K. & Kasagi, N. 2002 Highly energy-conservative finite differencemethod for the cylindrical coordinate system. *J. Comput. Phys.* **181**, 478–498.

Monte, S., Sagaut, P. & Gomez, T. 2011 Analysis of turbulent skin friction generated in flow along a cylinder. *Phys. Fluids* **23**.

Neves, J. C., Moin, P. & Moser, R. D. 1992 Numerical study of axial turbulent flow over long cylinder. *Tech. Rep.* 19920057442. NASA.

Ohta, T. 2017 Turbulence structures in high-speed air flow along a thin cylinder. *J. Turbul.* **6**, 497–511.

Piquet & Patal, V. C. 1999 Transverse curvature effects in turbulent boundary layer. *Progress in Aerospace Sciences* **35**, 661–672.

Woods, M. J. 2006 Computation of axial and near-axial flow over a long circular cylinder. PhD thesis, The University of Adelaide, Adelaide, South Australia.